Dyes and Pigments 209 (2023) 110905

Contents lists available at ScienceDirect

Dyes and Pigments

journal homepage: www.elsevier.com/locate/dyepig

Newly synthesized benzothiazolyl-1,2,3-triazole derivatives: Intramolecular charge transfer tuning, solvatofluorochromism and antiproliferative properties

Francisco J. Ballester [a], Enrique Ortega-Forte [a], Delia Bautista [b], M. Dolores Santana [a,**], Giampaolo Barone [c,***], José Ruiz [a,*]

[a] Departamento de Química Inorgánica, Universidad de Murcia, Biomedical Research Institute of Murcia (IMIB-Arrixaca), E-30071, Murcia, Spain
[b] SUIC-ACTI, Universidad de Murcia, E-30071, Murcia, Spain
[c] Dipartimento di Scienze e Tecnologie Biologiche, Chimiche e Farmaceutiche (STEBICEF), Università di Palermo, 90128, Palermo, Italy

ARTICLE INFO

Keywords:
Push-pull architecture
Solvatofluorochromism
ICT
Antitumor activity
1,2,3-triazole derivatives

ABSTRACT

A family of 6 new 1-aryl-4-benzothiazolyl-1,2,3-triazoles with CH_3, F, CF_3, NO_2, OCH_3 and $N(CH_3)_2$ substituents in the R4 of the phenyl ring has been prepared from the respective aldehyde treated with *ortho*-aminothiophenol. The compounds are characterized in solution using multinuclear NMR spectroscopy and in the solid state by X-ray diffraction. The emission spectra of the compounds with stronger electron-donating groups, OCH_3 and $N(CH_3)_2$, exhibit a red-shifted band (391 and 515 nm, respectively), the latest showing the largest Stokes shift and the highest quantum yield, which increases with the decrease polarity of the solvent. The excited-state lifetimes of all compounds showed a bi-exponential decay with a short (5–12 ns), according to an admixture of intramolecular charge transfer (ICT) and π-π*, and a long (45–100 ns) component. The calculated structures of their first singlet excited state by TD-DFT in acetonitrile (ACN) solution allows to estimate the change in the dipole moments, which explains the ICT character of their first singlet excited state for the NO_2 and $N(CH_3)_2$ derivatives. Important to note that compound with the electron-donating $N(CH_3)_2$ substituent showed strong solvatofluorochromism (correlated well with the ICT and the dipole moments). Interestingly, some of the compounds are active in human A2780, HeLa and A549 cancer cell lines, exhibiting IC_{50} values in the low micromolar range, whereas showing low cytotoxicity in healthy CHO cells. Important to note that the $N(CH_3)_2$ derivative showed cytoplasmic staining as determined by confocal fluorescent microscopy.

1. Introduction

The design of π-conjugated azaheterocyclic-based donor-acceptor type chromophores (push-pull architecture) has been the subject of intense research during the last decade because their photophysical properties can be easily modulated by external stimuli [1]. In this context, bicyclic heterocycles, like benzothiazole, act as moderate to strong electron-withdrawing groups. The molecules that incorporate this type of heterocycles as an attractor exhibit an intense positive solvatochromism in their emission (red-shift with increasing the polarity of the solvents), which indicates that they undergo an intramolecular charge transfer (ICT) when excited [2–4]. Many of these push-pull systems show appreciable photoluminescence. However, unlike absorption, fluorescent emission is significantly affected by the nature of the substituents. In compounds with moderately electron-donating groups (alkyl, alkyloxy, etc.) or electron-withdrawing groups (e.g. CF_3) only a moderate loss or even an increase in fluorescent intensity is occasionally observed, with a red shift of the emission band [5].

Benzothiazoles also represent privileged scaffolds in medicinal chemistry with many applications as anticancer agents [6–13], enzyme

Abbreviations: ICT, intramolecular charge transfer; MTT, 3-(4,5-dimethylthiazol-2-yl)-2,5-diphenyltetrazoliumbromide; MTG, MitoTracker Green; IC_{50}, concentration of the compound inhibiting cell growth by 50%.

* Corresponding author.
** Corresponding author.
*** Corresponding author.
E-mail addresses: dsl@um.es (M.D. Santana), Giampaolo.barone@unipat.it (G. Barone), jruiz@um.es (J. Ruiz).

https://doi.org/10.1016/j.dyepig.2022.110905
Received 9 September 2022; Received in revised form 15 October 2022; Accepted 1 November 2022
Available online 10 November 2022

inhibitors [14], antibacterial agents [15,16], anti-inflammatory [17], bioimaging agents [18–20], and antifungal agents [21]. Recently, different 2-arylbenzothiolate derivatives have shown anticancer activity against cervical cancer cell lines, HL-60 and U-937 [17]. The 5-fluorobenzothiazole prodrug (Phortress) is a suitable candidate for Phase I clinical trials [22].

On the other hand, the 1,2,3-triazole ring is a major pharmacophore system among nitrogen-containing heterocycles as antimicrobial [23,24], anticancer [25–27], anti-tubercular, antiviral, antidiabetic, antimalarial, anti-leishmanial, and neuroprotective agents [28]. Other interdisciplinary applications of 1,2,3-triazole scaffolds are related to different areas of science, such as homogeneous catalysis [29], coordination chemistry [30–32], and materials science [33]. Thus for example, 3-triazolylquinoxalines allow an excellent entry to tunable emission solvatochromic fluorophores with triazole ligation [34], and coumarin-triazoles exhibit an extraordinary utility in the photophysical and medicinal industries due to their fluorogenic activity [35–37].

In 2005 Bianchard-Desce and coworkers described for first time the association of an electron-donating and an electron-withdrawing connected by a triazole ring [38,39]. In 2008 Diederich et al. have described push-pull type chromophores containing 1,2,3-triazoles as π -linker fragments and the influence of isomeric charge transfer between the 1, 2.3-triazole fragment and the dicyanovinyl group on their optical properties [40]. Furthermore, Zych et al. have recently combined a terpyridine moiety with a (4-substituted)-1,2,3-triazol-1-yl ring at the 4-position of the phenyl ring of 4′-phenyl-2,2':6′,2″-terpyridine and have established the influence of the substituents on the optical and photophysical properties of the derivatives as well as their support with quantum-mechanical calculations based on DFT methods [41–43].

With this in mind, the aim of this article is synthesis, structure and optoelectronic properties of a series of new benzothiazolyl-1,2,3-triazole (BTAT) derivatives (compounds **5a-f** in Scheme 1.). Theorical calculations have been performed in order to rationalize the charge transfer (CT) character of relevant absorptions, the large Stokes shifts and solvatochromic behavior. The biological activity of the new BTAT towards numerous cancer cell lines have also been studied. The synthesis of some derivatives with a similar structure (5-methyl substituted) have previously been reported [44].

2. Results and discussion

2.1. Synthesis and characterization

The synthesis of the 2-(1-(aryl)-1,2,3-triazol-4-yl)benzothiazoles **5a-f** (Scheme 1) was initiated with the preparation of the previously reported aromatic azides **2a-f** [23] following a slight modification of established literature methods. The formation of the triazoles **3a-f** involved the 1,3-dipolar cycloaddition reaction between propargyl alcohol and the corresponding aromatic azide catalyzed by Cu(I). Then, the 1,2,3-triazole alcohols **3a-f** were further oxidized to 1,2,3-triazole-4-carbaldehydes **4a-f** using oxalyl chloride in DMSO. Finally, to synthesize the 1-aryl-4-benzothiazolyl-1,2,3-triazoles **5a-f**, the respective aldehydes (**4a-f**) were treated with 2-aminothiophenol, leading to the products as white solids in good yields (ranging from 60 to 80%), except in the case of compound **5d** that could not be obtained directly from the reaction.

Reagents and conditions: i) $NaNO_2$, HCl 6 M, H_2O, 0 °C, 1 h. ii) NaN_3, 2 h, r.t. iii) propargyl alcohol, 5% $CuSO_4{\cdot}5H_2O$, 10% sodium ascorbate. iv) $^tBuOH/H_2O$ (1:1), 72 h, r.t. v) $(COCl)_2$, DMSO, DCM anh., −78 °C, atm. N_2, 15 min. vi) Et_3N, −78 °C, atm. N_2, 15 min vii) 24 h, atm. N_2, r.t. viii) 5% CF_3COOH, EtOH, 24 h, r.t. ix) DDQ, DCM anh., 2 h. 0 °C.

Instead, the reduced form **6d** was generated, and an oxidation step was required to synthesize the desired compound **5d**. All compounds **5a-f** were fully characterized by ^1H NMR, ^{13}C NMR and high-resolution ESI-mass spectrometry and microanalysis (Figs. S1–S70, Supp Info). The high-resolution ESI mass spectra of the compounds **5a-f** showed the sodiated molecular ion $[M+Na]^+$ and $[M+H]^+$. The fragment $[M\text{-}2N + H]^+$ was observed as the more intense peak. In the ^1H NMR spectra, the resonances of the respective protons of the synthesized compounds were assigned on basis of their chemical shifts, multiplicities and coupling constants (Fig. 1). The triazole protons H_9 were observed as a singlet between 8.5 and 8.7 ppm. This resonance is sensitive to the substituent on the triazole fragment (see below).

The two protons adjacent to the thiazole ring (H_2 and H_5) show two resonances around 8 ppm as pseudo-doublets. The signals of the aromatic protons of the phenyl substituent (H_{11}, H_{12}, H_{14} and H_{15}), since they are equivalent two to two, were assigned easily. The resonances of H_{11}, H_{12}, H_{14} and H_{15} protons of such ring are very dependent on the nature of the R substituent, highly withdrawing substituents (NO_2, CF_3) lead to larger shifts while electron-donor substituents (OCH_3, $N(CH_3)_2$) lead to lower ones. The quaternary carbons are assigned by overlapping the spectrum of ^{13}C and DEPT-135 (see Supp Info). As shown in Fig. 2, there is a good correlation between chemical shift, experimental and theoretical, of H_9 proton of the triazole group and the Hammett constants of the R substituent (see below).

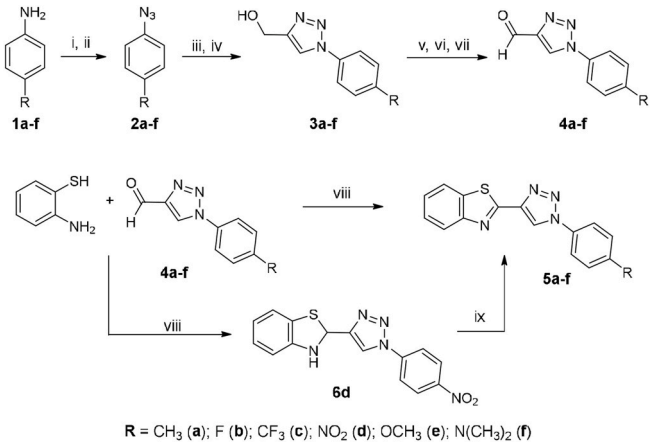

Scheme 1. Synthetic route for the preparation of 1,2,3-triazole derivatives.

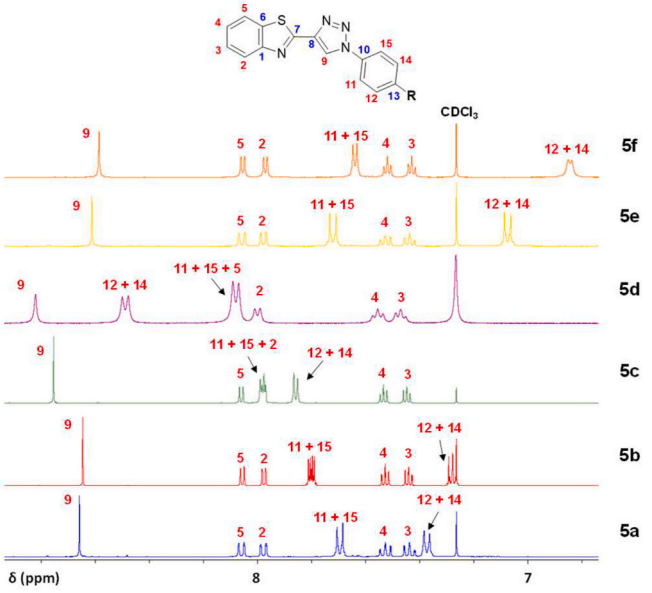

Fig. 1. Aromatic region of ^1H NMR of compounds **5a-f** in $CDCl_3$.

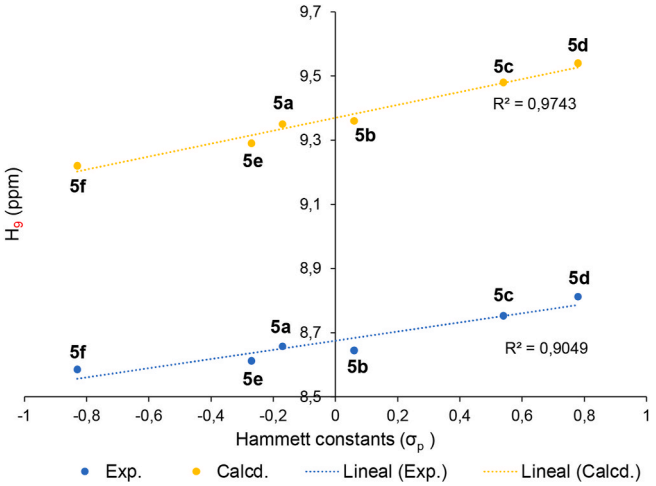

Fig. 2. Experimental and calculated chemical shifts of H_9 proton *versus* Hammett constants of the R substituent.

2.2. Solid-state structure

Suitable crystals of **5c** were obtained by slow evaporation of a solution in acetonitrile (ACN). The compound **5c** crystallizes in a monoclinic system, space group $P2_1/n$, with four molecules in the unit cell. The molecules in the unit cell are disposed antiparallel and rotated to each other (Fig. S83). Its X-ray molecular structure is depicted in Fig. 3.

Relevant interatomic distances, angles and torsional angles are listed in Tables S1–S3. The bond distances values N1–C7 of 1.304(2) Å and N1–C1 of 1.393(2) Å are in range for an N(sp^2)—C(sp^2) double and single bond order character, respectively, whereas C7–C8 bond distance of 1.459(3) has a value for a typical single Csp^2—Csp^2 bond [46]. Bond lengths values S1–C7 of 1.753(2) Å and S1–C6 of 1.730(2) Å are characteristic for a single S— Csp^2 bond. The N2–N3 bond length of 1.304(2) Å is shorter than that expected for an N–N single bond (1.42 Å) [47], while the two C–N bond lengths (C8–N2, 1.367(3) Å and C9–N4, 1.357 (2) Å), involving the triazole ring are between the characteristic single (1.42 Å) and double bond lengths (1.27 Å) [48]. The molecule is not planar because of the twisting of the benzothiazole ring system and the triazole unit. Thus, the dihedral angle between them (N1–C7–C8–C9) is −15.6(3)°.

As well as, the dihedral angle between the triazole ring and the 4-(trifluoromethyl)phenyl unit (C9–N4–C10–C11) is 17.1(3)° (Fig. S84). Theoretical calculations have been carried out in ACN solution to obtain information on the structure and electronic properties of compounds **5a-f**. The optimized geometries of their most stable conformations are shown in Fig. 4 and their conformations are in excellent agreement with that of the experimental structure of **5c** (Fig. 3). A second conformation for each compound was found, in which the S atom and the H_9 atoms are cis, are reported in supplementary (Fig. S85) and are more than 10 kJ/mol less stable. The structures shown in Fig. 4 have also been used to obtain the calculated ^{1}H NMR chemical shift values of the H_9 atom in ACN solution, reported in Fig. 2.

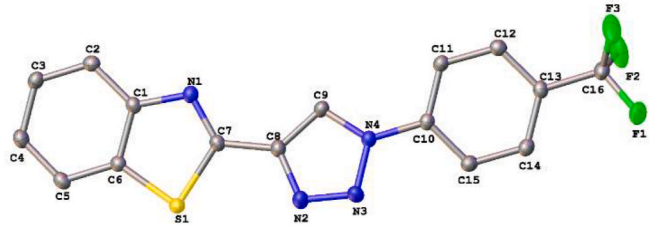

Fig. 3. X-ray crystal structure of **5c** with atom labeling scheme. ORTEP view at 50% probability level. Hydrogens have been omitted for clarity.

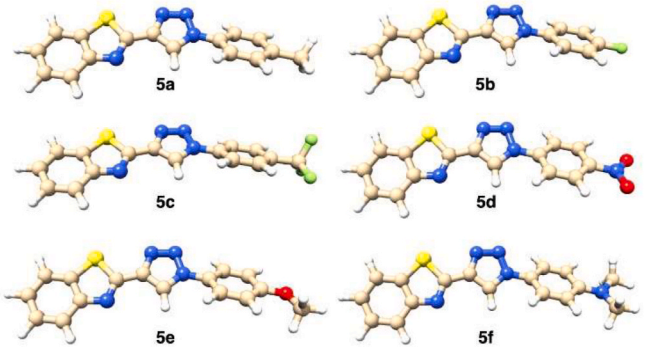

Fig. 4. Structures of the compounds **5a-f** obtained by DFT calculations in ACN solution.

2.3. Absorption properties

The absorption spectra of compounds were carried in ACN solutions (5×10^{-5} M) at room temperature, data are shown in Table 1. The absorption spectra of compounds **5a-f** show an intense absorption band with a shoulder in the region between 250 and 330 nm with molar extinction coefficients around 20000 M^{-1} cm^{-1} (Fig. 5). In general, the absorption spectra of compounds **5a-f** are characterized by bands assigned mainly to the π-π* transition the aromatic system of the triazole fragment and the benzothiazole moiety. In Fig. 5 (top) we show the observed electronic absorption spectra of compounds **5a-f**.

As can be seen from Fig. 5, the absorption maxima depend on the low or moderately electron-donating (CH_3, OCH_3) or electron-withdrawing substituent groups (F, CF_3) in the triazole fragment that are blue-shifted instead of compounds **5d** and **5f** with strong electron-withdrawing (NO_2) or electron-donating substituent ($N(CH_3)_2$), respectively, show red-shifted maxima.

It is interesting to note that the lowest energy experimental absorption bands and trends (Fig. 5 top) are nicely reproduced by the theoretical spectra obtained by TD-DFT calculations (Fig. 5 bottom)

The wavelength, oscillator strength and composition of the first two significant absorption peaks of compounds **5a-f** are listed in Table 2 (see also Fig. 5, bottom). In particular, the most intense absorption peak is also the lowest energy peak, and involves essentially a HOMO-LUMO electronic transition for all six compounds **5a-f**.

The analysis of the HOMO and LUMO (Fig. S86) allows us to conclude that such transition can be described as a charge-transfer band only for compounds **5d** and **5f** since it corresponds to a shift of the involved electron from the benzothiazole moiety to the substituted

Table 1
Optical properties data for compounds **5a-f** in ACN solution at r.t.

Compound	λ_{abs}/nm (ε/M^{-1} cm^{-1})	λ_{em} (λ_{ex})/nm	Stokes/ cm^{-1}	Φ_F[a,b]	τ[b]/ns (%)
5a	226 (26312) 293 (22594)	361 (300)	6429	0.02	6.2 (48) 63.9 (52)
5b	227 (25224) 292 (19544)	360 (290)	6469	0.01	5.8 (20) 50.0 (80)
5c	225 (27960) 295 (15348	365 (300)	6501	0.01	5.2 (20) 53.5 (80)
5d	221 (21372) 311 (20974)	375 (300)	5588	<0.01	12.8 (34) 45.4 (66)
5e	224 (12158) 292 (12002)	391 (300)	8671	0.08	3.6 (26) 69.7 (74)
5f	224 (25670) 320 (27302)	515 (315)	11833	0.19	6.2 (67) 99.9 (33)

[a] Ref. Cou314 (Φ_F = 0.68 at EtOH) [45].
[b] Under nitrogen atmosphere.

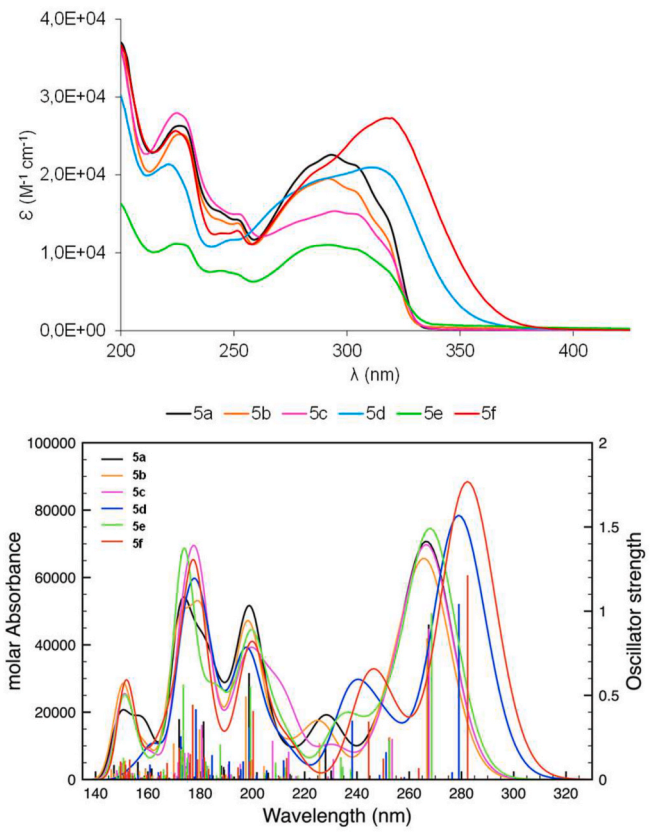

Fig. 5. Experimental (top) and calculated (bottom) electronic absorption spectra of compounds **5a-f** in ACN solution.

Table 2
Absorption wavelength (λ, nm), oscillator strength (f) and major contributions of occupied and virtual molecular orbitals (H: HOMO, L: LUMO), of the lower energy absorption transitions of compounds **5a-f**, obtained by TD-DFT calculations in ACN solution (see Fig. 5, bottom).

Compound	Transition	λ (nm)	f	Major contributions (%)
5a	$S_0 \rightarrow S_1$	267.46	0.92	H→L (83)
	$S_0 \rightarrow S_2$	252.36	0.25	H-1→L (70)
5b	$S_0 \rightarrow S_1$	266.79	0.84	H→L (82)
	$S_0 \rightarrow S_2$	252.50	0.25	H-1→L (69), H→L (11), H→L+3 (10)
5c	$S_0 \rightarrow S_1$	267.58	0.89	H→L (71), H→L+1 (12)
	$S_0 \rightarrow S_2$	253.47	0.24	H-1→L (51), H-1→L+1 (22), H→L (11)
5d	$S_0 \rightarrow S_2$	279.00	1.04	H→L (53), H-2→L (14), H→L+1 (24)
	$S_0 \rightarrow S_5$	251.14	0.16	H→L+1 (55), H-2→L (10), H-1→L (11), H-1→L+1 (11)
5e	$S_0 \rightarrow S_1$	268.61	0.99	H→L (71), H-2→L (17)
	$S_0 \rightarrow S_2$	252.42	0.23	H-2→L (40), H-1→L (34)
5f	$S_0 \rightarrow S_1$	282.36	1.21	H→L (56), H-1→L (21), H→L+1 (18)
	$S_0 \rightarrow S_4$	250.11	0.12	H-2→L (43), H-1→L (22), H→L+1 (22)

phenyl group (**5d**) or, in the opposite way, from the substituted phenyl group to the benzothiazole fragment (**5f**). For compounds **5a-c** and **5e**, the HOMO and LUMO are located almost over the same region of the structure so the low-lying absorption band for these compounds can be described as a π-π* transition.

In **5d** and **5f** with strong electron-withdrawing or electron-donor substituents, respectively, the HOMO and LUMO are essentially in the opposite region of the molecule, only sharing the 1,2,3-triazole ring. It is remarkable how the electronic properties of the benzothiazole ring are modified (Fig. 6) [49]. In compound **5f**, HOMO is located in the electron-rich region of the structure, the phenyl ring with the $N(CH_3)_2$ substituent, and LUMO is in the benzothiazole region. When the phenyl ring contains the strong electron-withdrawing NO_2 substituent in **5d**, the benzothiazole fragment behaves as an electron-donor system and the HOMO is located over this ring, while the LUMO is located in the substituted phenyl ring. Interestingly, for compounds **5d** and **5f** the first electronic transition occurs at lower energy (279 and 282 nm, respectively), while for the remaining compounds the analogous transition occurs at a slightly higher energy (around 267–269 nm, see Table 2).

Figure S87 shows, for compounds **5a-f**, the absolute values (in a.u.) of the HOMO and LUMO energy levels and the energy difference (in kJ/mol) between them. In this plot, independently of the electron-donor or electron-withdrawing nature of the substituents, it is seen that **5a**, **5b**, **5c** and **5e** have approximately the same values of both HOMO and LUMO calculated energies and very similar energy difference between them (in the range 652–662 kJ/mol). On the other hand, the electron-withdrawing NO_2 group in **5d** induces a stabilization of the LUMO, so decreasing the HOMO-LUMO energy difference to 574 kJ/mol while the electron-donor $N(CH_3)_2$ group in **5f** induces destabilization of the HOMO, so decreasing the energy difference to about 576 kJ/mol.

2.4. Emission properties

The emission properties of all compounds have been studied in ACN solutions. Compounds **5a-d** show an unstructured band in the blue region between 360 and 390 nm (Table 1) and compounds **5e** and **5f** which contain stronger electron-donating groups, OCH_3 and $N(CH_3)_2$, exhibit a red-shifted band at 391 and 515 nm, respectively [42,43,50]. A plausible explanation could be that the introduction of electron-withdrawing substituents stabilizes the energy levels of both HOMO and LUMO. In contrast, electron-donating groups, destabilize the energy levels of both HOMO and LUMO [41,42,49]. In this way, the transition energy remains essentially the same. Also, compound **5f** shows the largest Stokes shift. The corresponding spectra are shown in Fig. 7.

Compounds **5a-d** exhibit low fluorescence quantum yields (Table 1), even **5d** is almost non-emissive with Φ_F less than 0.01, perhaps due to inhibition of fluorescence by the $-NO_2$ group [51]. However, compound **5f** has the highest quantum yield, which increase with the decrease polarity of the solvent (see below, Table 3 and Fig. 8). Time-correlated single photon counting (TCSPC) measurements yield to the excited-state lifetimes of all compounds which show a bi-exponential decay with a short (5–12 ns) and a long (45–100 ns) component. The bi-exponential intensity decays can be according to an admixture of ICT and π-π* transitions. To support the observed ICT character of the emission bands of compounds **5a-f**, we have represented their HOMO and LUMO in supplementary (Fig. S86). Moreover, we have calculated the structure of their first singlet excited state by TD-DFT in ACN solution (Fig. S88) to estimate the change in dipole moment occurring following the electronic transition. Interestingly, in the excited state structures the benzothiazole and phenyl rings are more coplanar. The data obtained are shown in Table 4 and it is possible to see that the dipole moment decreases for compounds **5a-c** and **5e**, while it increases for **5d** and **5f**. Such trend well explains the ICT character of their first

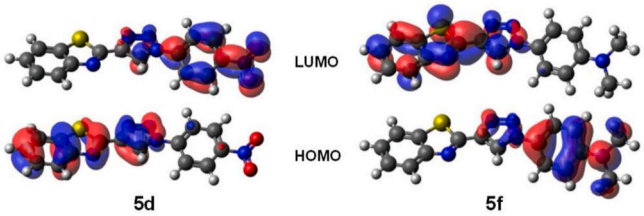

Fig. 6. HOMO and LUMO of **5d** and **5f**.

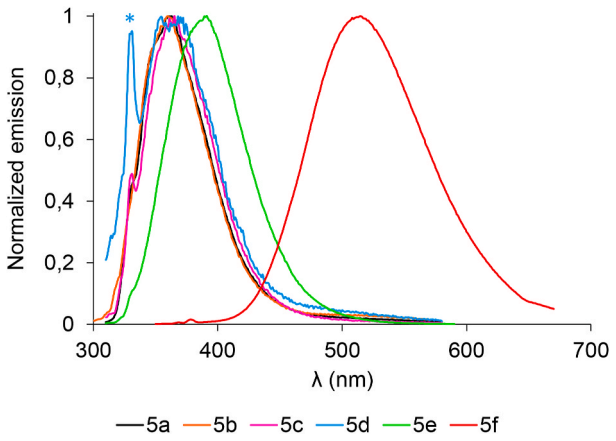

Fig. 7. Normalized emission spectra of compounds **5a-f** in ACN solution. Peak marked with * is an artifact.

Table 3
Optical properties **5f** in solid and in various solvents at r.t.

	λ_{abs}/nm (ε/M^{-1} cm^{-1})	λ_{em} (λ_{ex})/ nm	Stokes/ cm^{-1}	Φ_F[a,b]	τ[b]/ns (%)
Solid	–	454 (270)	–	–	–
Toluene	323 (28890)	415 (290)	6863	0.56	10.0 (40) 54.1 (60)
Chloroform	323 (27680)	437 (300)	8077	0.27	4.6 (38) 87.6 (62)
Ethanol	322 (30740)	518 (300)	11751	0.16	4.2 (35) 85.0 (65)
ACN	320 (27302)	515 (315)	11833	0.19	6.2 (67) 99.9 (33)
DMSO	322 (27080)	525 (315)	12008	0.17	7.0 (80) 86.2 (20)

[a] Ref. Cou314 (Φ_F = 0.68 at EtOH) [45].
[b] Under nitrogen atmosphere.

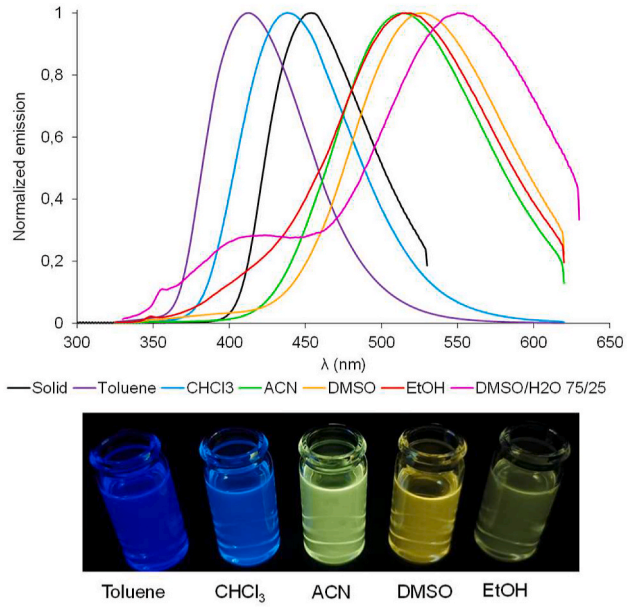

Fig. 8. Top: normalized emission spectra of compound **5f** in solid and in different solvents. Bottom: image of the emission of **5f** in different solvents (λ_{ex} = 312 nm).

Table 4
Dipole moments (Debye) of compounds **5a-f** in the ground state (μ_{GS}) and in the first excited state μ_{1ES}, and their difference ($\mu_{1ES} - \mu_{GS}$), obtained by DFT and TD-DFT calculations, respectively, in ACN solution.

Compound	μ_{GS}	μ_{1ES}	μ_{1ES} - μ_{GS}
5a	5.14	4.93	−0.21
5b	3.64	3.24	−0.40
5c	3.38	2.85	−0.53
5d	4.47	6.32	1.85
5e	6.38	6.26	−0.11
5f	7.64	8.08	0.43

singlet excited state, as inferred on the basis of their HOMO and LUMO (Fig. 6).

To gain insight into the ICT character of the excited state, emission spectra of compounds **5c**, **5e** and **5f** in different solvents at room temperature have been further studied (Fig. 8, Figs. S73–S74 and Table 3). The large and positive solvatochromism as well as the sensitivity of the emission intensity indicate a considerable ICT characteristic of the compounds [52].

Compound **5c** does not exhibit solvatochromism (Fig. S73) and neither does it show an increase in the dipole moment in the excited state (Table 4). Compound **5e** (Fig. S74) shows a slight solvatochromism, whereas compound **5f** shows a strong solvatochromic behavior. Thus, by increasing the polarity of the solvent, e.g., toluene, chloroform, ethanol, ACN and DMSO the emission maxima shift to the red λ_{em} = 415, 437, 518, 515, and 525 nm, respectively. This strong solvatochromic behavior is in agreement with the pronounced CT character of the excited state, as confirmed by calculations (see below). Moreover, as the polarity of the solvent increases the emission intensity and the fluorescence quantum yields decrease (Φ_F, toluene = 0.56, Φ_F, DMSO = 0.17).

The decrease in the fluorescence quantum yield is common for compounds with strong ICT character [53,54]. In the other hand, compound **5c** with less ICT character of the excited state do not show this emission maxima redshift with the increase of the solvent polarity (Fig. S73). In order to study the emission behavior of **5f**, emission spectra of solution of **5f** in different mixtures of DMSO/H_2O were recorded (Fig. 9). With small increases of the water proportion, the intensity of the emission band at 525 nm decreases and the maxima gets redshifted. At equal proportion DMSO/H_2O, the emission of **5f** was quenched, as in the mixture 1/3 (v/v) DMSO/H_2O. When the water

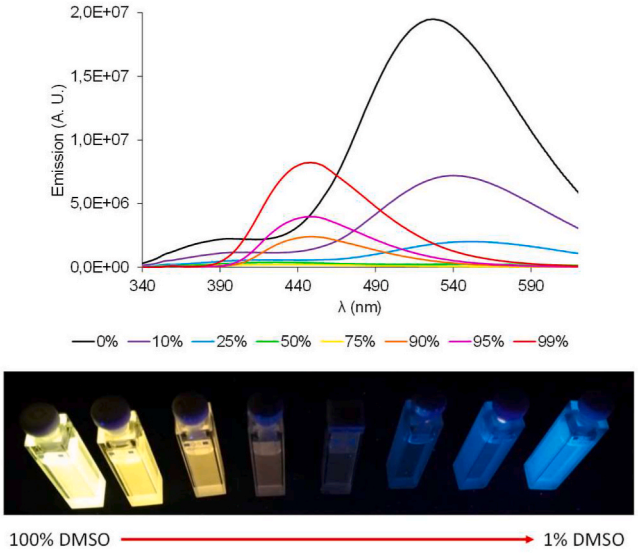

Fig. 9. Top: emission spectra of compound **5f** (10 μM) in mixtures DMSO/H_2O with increasing water proportion. Bottom: image of the samples under UV irradiation (λ_{ex} = 320 nm).

percentage reaches 90% of the mixture, a new emission band was observed at higher energy, and its intensity and emission maxima blueshift got increases with the water proportion. This higher energy band could be explained with the aggregation of the molecules of **5f** or it can be attributed to either aggregation induced emission (AIE) or crystalline induced emission (CIE) as the proportion of water increases. Similar behavior has been observed in systems where the crystallization leads to enhanced emission [55].

To determinate if **5f** aggregated in solutions with high water proportions, the ^{1}H NMR spectra of samples of **5f** (1 mM) with different proportions of DMSO-d_6/D_2O were recorded. The results showed that the compound began to precipitate when the water percentage reached 33% and the precipitate could be observed at bare eye (Fig. 10, bottom). Also, resonance of the H_9 proton gets displaced to lower chemical shift with the increase of water proportion in the mixture.

2.5. Antiproliferative activity

Once the optical properties were determined, the antiproliferative activities of the present compounds were evaluated against a panel of human cancer cells including ovarian cancer cells (A2780), cervix adenocarcinoma (HeLa) and lung carcinoma epithelial cells (A549). Moreover, a non-tumorigenic ovarian cell line (CHO) was used to evaluate selectivity of the compounds towards tumoral cells over normal cells. The clinical drug cisplatin was used as a reference for anticancer evaluation. As shown in Table 5 and Fig. S89, the compounds exerted moderate to high antiproliferative activity in A2780 and HeLa cancer cells, with half-maximal inhibitory concentration (IC_{50}) values in the low micromolar range, whereas mild to minimal toxicity was observed in A549 cells; the IC_{50} values being markedly higher. Interestingly, normal ovarian CHO cells were not affected by these compounds up to 100 μM in contrast to cisplatin, which delivered strong cytotoxicity towards these cells. This might point out a preferential selectivity of these compounds towards cancer cells, although further research will be needed to prove this assumption. Compared to HeLa cell line, the higher anticancer activities were found in A2780 cells. Overall, **5c**, **5d** and **5f** were the most active agents with higher selectivity factors (SF). Although the mechanism of action of these compounds needed further investigation, it seems that the more active molecules are those containing either moderate or strong electron withdrawing (CF_3, NO_2) or strong electron-donating $N(CH_3)_2$ substituents. Regarding to anticancer

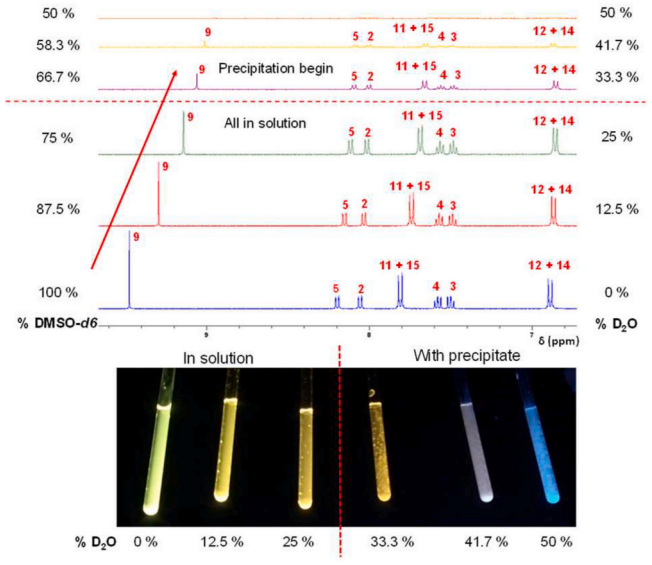

Fig. 10. Top: aromatic region of ^{1}H NMR spectra of **5f** (1 mM) solutions in different DMSO-d_6/D_2O mixtures. Bottom: image of the samples under UV irradiation (λ_{ex} = 312 nm).

Table 5
IC_{50} values [μM] after 48 h treatment with compounds **5a-f** and cisplatin.[a]

Compound	A2780	HeLa	A549	CHO	Selectivity factor.[b]
5a	22 ± 2	32 ± 4	17 ± 2	>100	>4.5
5b	>100 [83% ± 6]	5.9 ± 0.4	>100	>100	–
5c	7.2 ± 0.9	36 ± 5	>100	>100	>13.8
5d	5.5 ± 0.8	23 ± 2	>100	>100	>18.2
5e	11 ± 2	46 ± 4	54 ± 4	>100	>9.1
5f	14 ± 2	10.0 ± 0.9	21 ± 1	>100	>7.1
Cisplatin	1.9 ± 0.1	21 ± 2	39 ± 4	7.8 ± 0.4	4.1

[a] Cell viability determined by MTT assays represented as mean ± SD of three independent experiments. The term >100 indicates that no IC_{50} was found up to that concentration. If significant difference was observed at 100 μM, the respective percentage of inhibition is given in parentheses.
[b] Selectivity factor calculated as IC_{50}[normal CHO]/IC_{50}[tumoral A2780].

effects, contrast-phase microscopy revealed that the compounds could exert cytotoxicity to cancer cells which resulted in rounded and detached cells, an indicative of cell death induction (Figs. S90 and S91).

2.6. Cellular uptake and localization of 5f

The emission properties of compound **5f** allowed us to track its uptake and localization inside cancer cells. HeLa cells were incubated with the compound for 1 h and imaged using confocal microscopy. As shown in Fig. 11 and Fig. S92, compound **5f** was able to internalize into living cancer cells, thereby emitting intracellular fluorescence. Strikingly, the fluorescence of the compound was observed evenly distributed around cell cytoplasm but not within nuclei, which suggest that nuclear DNA was not likely to be the main target. In fact, the cytoplasmic localization may indicate that, in contrast to platinum-anticancer drugs such as cisplatin, these compounds may exert their anticancer activity through

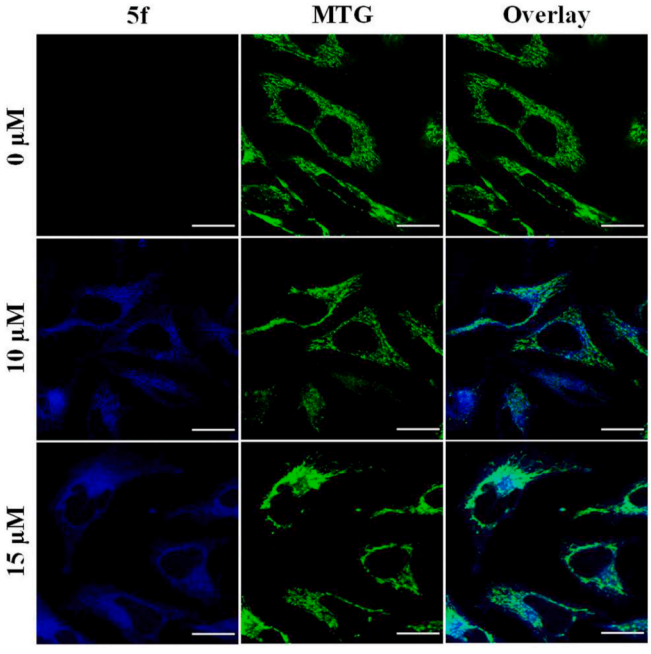

Fig. 11. Confocal microscopy images of HeLa cancer cells treated with **5f** at indicated concentrations for 1 h and co stained with 100 nM of mitochondrial dye. $\lambda_{ex}/\lambda_{em}$: 405/450 nm for **5f**; 488/530 nm for MitoTracker Green (MTG). Scale bar: 20 μm.

interaction with proteins and biomolecules in the cytosol. In addition, co-localization studies were carried out using MitoTracker Green (MTG) for mitochondria.

As observed in Fig. 11, confocal imaging showed that **5f** fluorescence was partially overlapped with that generated by MTG. However, **5f** fluorescence was observed in the whole cytoplasm. The Pearson correlation coefficient of the green and blue fluorescence signals from MTG and **5f** respectively was 0.38, thus indicating a partial co-localization with MTG. Therefore, we hypothesize that one of the targets of **5f** action could be mitochondria, although this compound might accumulate in other subcellular organelles.

3. Conclusions

We have prepared a series of six BTAT derivatives. The compounds are characterized in solution using multinuclear NMR spectroscopy and in the solid state by X-ray diffraction. The synthesized donor-acceptor molecules exhibit optical properties based on charge-transfer emission depending on the substituent in the 1,2,3-triazole moiety. If we consider the HOMO and LUMO orbitals as representative of the ground and of the first excited state wave functions, respectively, a partial explanation of the fact that **5a**, **5b**, **5c** and **5e** have approximately the same position of absorption and emission maxima, can be provided by the plot reporting in Fig. S87. Thus, independently of the electron-donor or electron-withdrawing nature of the substituents, it is seen that **5a**, **5b**, **5c** and **5e** have approximately the same values of both HOMO and LUMO calculated energies and very similar energy difference between them. On the other hand, the electron-withdrawing NO_2 group in **5d** induces a stabilization of the LUMO, so decreasing the HOMO-LUMO energy difference while the electron-donor $N(CH_3)_2$ group in **5f** induces destabilization of the HOMO, decreasing the energy difference. This compound with the electron-donating $N(CH_3)_2$ substituent showed moderate photoluminescence quantum yield that increased with the decrease polarity of the solvent as well as strong solvatochromic behavior due to an intramolecular charge transfer excited-state. DFT and TD-DFT modeling indicates that the character of the lowest energy excitation changes upon the substitution on the triazole moiety.

The cytotoxic activities obtained for compounds **5a-f** vary according to the cell line studied. Thus they showed moderate to high antiproliferative activity in A2780 and HeLa cancer cells, with IC_{50} values in the low micromolar range, whereas mild to minimal toxicity was observed in A549 cells. All compounds do not present appreciable toxicity on no tumorigenic CHO cell line, that is an asset for further applications.

The emission properties of compound **5f** allowed us to track its uptake and localization inside cancer cells. HeLa cells were incubated with **5f** which was able to internalize into living cancer cells, thereby emitting intracellular fluorescence. Strikingly, the fluorescence of the compound was observed evenly distributed around cell cytoplasm but not within nuclei, which suggest that nuclear DNA was not likely to be its target.

4. Experimental section

4.1. General methods

All chemicals were of reagent grade and were used without further purification. When necessary, solvents were dried and distilled by general methods before use. The ^1H and ^{13}C NMR spectra were recorded on Bruker AC 300E, Bruker AV 400, or Bruker AV 600 NMR spectrometer. Chemical shifts are cited relative to $SiMe_4$ or by reference to the residual ^1H and ^{13}C solvent peaks. The ^{19}F NMR spectra were recorded on Bruker AC 200, and the chemical shifts were determined by reference to trifluoroacetic acid ^{19}F NMR resonance. UV/Vis spectroscopy was carried out on a PerkinElmer Lambda 750 S spectrometer and FT-IR spectroscopy was carried out on a PerkinElmer 1430. ESI mass (positive mode) analyses were performed on a HPLC/MS TOF 6220. Excitation and emission spectra were recorded on a Jobin Yvon Fluorolog 3–22 spectrofluorometer with a 450 W xenon lamp double-grating mono-chromators and a TBX-04 photomultiplier. The solution measurements were carried out in a right-angle configuration using 10 mm quartz fluorescence cells. Lifetimes were measured using an IBH FluoroHub TCSPC controller and a NanoLED pulse diode excitation source; the estimated uncertainty is ± 10%. The C, H, N and S analyses were performed with a LECO CNHS-932 microanalyzer.

4.2. General procedure to synthetize (1-(aryl)-1,2,3-triazol-4-yl) methanol *3a-f*

The synthesis of compounds **3a-f** were performed as previously described [23]. Amine **1a-f** (10 mmol) was added to a 100 mL round bottom flask in an ice-bath with 10 mL of HCl aq 6 M. When the mixture reaches 0 °C, 20 mL of $NaNO_2$ solution (1.5 eq, 15 mmol, 1.035 g) was added drop by drop. The reaction was stirred 1 h at 0 °C. Then, 30 mL of a solution of NaN_3 (2 eq, 20 mmol, 1.3 g) and the mixture was stirred at 0 °C for 15 min and 2 h at r.t. An extraction to the crude of reaction was performed with AcOEt (4 x 20 mL), the organic phases were dried with $MgSO_4$ (anh.), filtered, concentrated and the crude of reaction was purified by flash chromatography column in silica, using as eluent a mixture of AcOEt/Hexane, yielding the respective product **2a-f** (Yields = 50–85%).

The corresponding azide **2a-f** (8 mmol) was dissolved in 16 mL of a mixture 1:1 $^tBuOH/H_2O$. Then propargylic alcohol (1.1 eq, 8.8 mmol, 493.3 mg), $CuSO_4{\cdot}5H_2O$ (5%, 0.4 mmol, 117.9 mg) and sodium ascorbate (10%, 0.8 mmol, 158.5 mg). The mixture was stirred for 72 h in the dark. Then, an extraction to the reaction crude was performed with DCM (4 x 100 mL), the organic phases were dried with $MgSO_4$ (ahn.), the solvent was removed under reduced pressure and the crude was purified by a short flash chromatography column in silica with a mixture of AcOEt/Hexane 8/2 as eluent, obtaining the desired 1,2,3-triazoles **3a-f**. The final yield of the desired 1,2,3-triazoles are between 56 and 72%.

(*1-(4-(dimethylamino)phenyl)-1H-1,2,3-triazol*-4-yl)*methanol* ***(3f)***. Grey powder. Yield = 68% (1.19 g). ^1H NMR (401 MHz, DMSO-d_6): = 8.46 (s, 1H), 7.64 (d, J = 9.1 Hz, 2H), 6.84 (d, J = 9.1 Hz, 2H), 5.27 (s, 1H), 4.58 (s, 2H), 2.96 (s, 6H). $^{13}C\{^1H\}$ NMR (101 MHz, DMSO-d_6): 150.2(C), 148.6(C), 126.4(C), 121.1(CH), 120.6(CH), 112.4(CH), 55.0 (CH_2), 40.0 (CH_3). HRMS (ESI/Q-TOF) *m/z*: $[M+H]^+$ Calcd for $C_{11}H_{15}N_4O$ 219.1240; Found 219.1239. HRMS (ESI/Q-TOF) *m/z*: $[M-2N-OH]^+$ Calcd for $C_{11}H_{13}N_2$ 173.1077; Found 173.1069. HRMS (ESI/Q-TOF) *m/z*: $[M+Na]^+$ Calcd for $C_{11}H_{14}N_4ONa$ 241.1060, Found = 241.1057. Anal. Calcd for $C_{11}H_{14}N_4O$: C, 60.53; H, 6.47; N, 25.67. Found: C, 60.34; H, 6.42; N, 25.79.

4.3. General procedure for synthetize 1-aryl-1,2,3-triazole-4-carbaldehydes *4a-f*

Compounds **4a-f** were synthetized by Swern oxidation of the respective alcohol **3a-f**. In a 250 mL dry two-neck round flask, three cycles of vacuum-N_2 were performed. 50 mL of dry DCM and oxalyl chloride (1.3 eq, 13 mmol, 1.65 g) were added, the mixture was cooled to −78 °C and then DMSO (1.33 eq, 13.3 mmol, 1.04 g) was added and was stirred for 15 min. In other dry flask, the respective alcohol **3a-f** (1 eq, 10 mmol) was dissolved in 100 mL of dry DCM and was cooled to −78 °C under nitrogen. This solution of **3a-f** was added to the reaction flask with a Teflon cannula and the reaction mixture was stirred at −78 °C for another 15 min, then Et_3N (5 eq, 50 mmol, 5.06 g) was added, and this mixture was stirred for 15 min at −78 °C and 24 h at r.t. Then, 150 mL of saturated $NaHCO_3$(aq) solution was added, and the reaction crude was transferred to a 500 mL extraction funnel. The crude of reaction was extracted with DCM (3 x 100 mL), dried with $MgSO_4$ (anh.) and the solvent was removed under reduced pressure, yielding the desired aldehydes **4a-f** (67–92%) Experimental NMR values are in agreement with the previously reported in literature [56].

4.4. General procedure for synthetize 2-(1-(aryl)-1H-1,2,3-triazol-4-yl) benzo[d]thiazoles **5a-f**

The aldehydes **4a-f** (5 mmol), ortho-aminothiophenol (1.1 eq, 5.5 mmol, 1.09 g) and trifluoroacetic acid (0.05 eq, 0.25 mmol, 28.5 mg) were dissolved in 100 mL of ethanol. The mixture was stirred for 24 h at r.t. A white solid precipitate appeared. The solid was filtered, washed with 5 mL of EtOH, and dried under vacuum, yielding the desired products without requirement of futher purification steps.

For aldehyde **4d**, a yellow solid **6d** was obtained and identified as the 2,3-dihydrobenzo[d]thiazole intermediate. To obtain the desired product **5d**, the compound **6d** (2 mmol, 650 mg) was dissolved in 150 mL of DCM at 0 °C. Then, DDQ (1.1 eq, 2.2 mmol, 0.5 g) was dissolved in other 100 mL of DCM, and then was slowly added to the reaction mixture, that was stirred for 2 h at 0 °C. Then, the organic phase was extracted with 4 x 120 mL of H_2O, dried with $MgSO_4$ (anh.) and the solvent was removed under reduced pressure. The solid was washed with 5 mL of methanol and 2 mL of diethyl ether, yielding **5d** as a white solid.

4.5. 2-(1-(p-tolyl)-1H-1,2,3-triazol-4-yl)benzo[d]thiazole (**5a**)

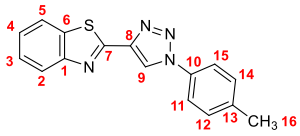

White powder. Yield = 80% (1.17 g). ^{1}H NMR (401 MHz, $CDCl_3$): 8.66 (s, 1H, H_9), 8.06 (ddd, J = 8.2, 1.2, 0.6 Hz, 1H, H_5), 7.98 (ddd, J = 7.9, 1.3, 0.6 Hz, 1H, H_2), 7.72–7.67 (m, 2H, H_{11} + H_{15}), 7.53 (ddd, J = 8.3, 7.1, 1.3 Hz, 1H, H_4), 7.44 (ddd, J = 8.2, 7.1, 1.2 Hz, 1H, H_3), 7.40–7.34 (m, 2H, H_{12} + H_{14}), 2.46 (s, 3H, H_{16}). ^{13}C{^{1}H} NMR (101 MHz, $CDCl_3$): 159.3(C_7), 153.8(C_1), 144.0(C_8), 139.8(C_{13}), 134.9(C_6), 134.5(C_{10}), 130.6(C_{12} + C_{14}), 126.6(C_4), 125.7(C_3), 123.1(C_5), 122.1 (C_2), 120.7(C_{11} + C_{15}), 120.1(C_9), 21.3(C_{16}). HRMS (ESI/Q-TOF) m/z: $[M+H]^+$ Calcd for $C_{16}H_{13}N_4S$: 293.0855; Found 293.0866. HRMS (ESI/Q-TOF) m/z: $[M-2N + H]^+$ Calcd for $C_{16}H_{14}N_2S$ 265.0794, Found 265.0803. HRMS (ESI/Q-TOF) m/z: $[M+Na]^+$ Calcd for $C_{16}H_{12}N_4SNa$ 315.0675, Found 315.0686. Anal. Calcd for $C_{16}H_{12}N_4S$: C, 65.73; H, 4.14; N, 19.16; S, 10.97. Found: C, 65.80; H, 4.08; N, 19.00; S, 11.03.

4.6. 2-(1-(4-fluoropheny)-1H-1,2,3-triazol-4-yl)benzo[d]thiazole (**5b**)

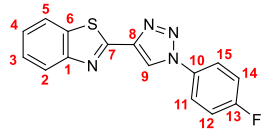

White powder. Yield = 60% (889 mg). ^{1}H NMR (600 MHz, $CDCl_3$): 8.65 (s, 1H, H_9), 8.06 (ddd, J = 8.2, 1.2, 0.6 Hz, 1H, H_5), 7.98 (ddd, J = 8.0, 1.2, 0.6 Hz, 1H, H_2), 7.82–7.77 (m, 2H, H_{11} + H_{15}), 7.53 (ddd, J = 8.3, 7.2, 1.2 Hz, 1H, H_4), 7.44 (ddd, J = 8.2, 7.2, 1.2 Hz, 1H, H_3), 7.31–7.25 (m, 2H, H_{12} + H_{14}). ^{13}C {^{1}H} NMR (101 MHz, $CDCl_3$): 162.8 (d, $J_{C,F}$ = 249.8 Hz, C_{13}), 158.9(C_7), 153.7(C_1), 144.1(C_8), 134.9(C_6), 133.0(C_{10}), 126.6(C_4), 125.7(C_3), 123.2(C_5), 122.8 (d, $J_{C,F}$ = 8.9 Hz, C_{11} + C_{15}), 122.1(C_2), 120.3(C_9), 117.2 (d, $J_{C,F}$ = 22.9 Hz, C_{12} + C_{14}). ^{19}F {^{1}H} NMR (188 MHz, ACN-d_3): −112.01. HRMS (ESI/Q-TOF) m/z: $[M+H]^+$ Calcd for $C_{15}H_{10}FN_4S$ 297.0605; Found 297.0608. HRMS (ESI/Q-TOF) m/z: $[M-2N + H]^+$ Calcd for $C_{15}H_{10}FN_2S$ 269.0543; Found 269.0548. HRMS (ESI/Q-TOF) m/z: $[M+Na]^+$ Calcd for $C_{15}H_9FN_4SNa$ 319.0424; Found 319.0429. Anal. Calcd for $C_{15}H_9FN_4S$: C, 60.80; H, 3.06; N, 18.91; S, 10.82. Found: C, 60.36; H, 2.93; N, 18.91; S, 10.93.

4.7. 2-(1-(4-(trifluoromethyl)phenyl)-1H-1,2,3-triazol-4-yl)benzo[d] thiazole (**5c**)

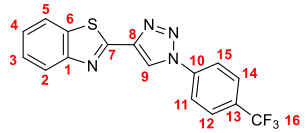

White powder. Yield = 68% (1.18 g). ^{1}H NMR (600 MHz, $CDCl_3$): 8.75 (s, 1H, H_9), 8.06 (ddd, J = 8.2, 1.1, 0.6 Hz, 1H, H_5), 8.01–7.96 (m, 3H, H_2 + H_{11} + H_{15}), 7.90–7.83 (m, 2H, H_{12} + H_{14}), 7.53 (ddd, J = 8.3, 7.2, 1.2 Hz, 1H, H_4), 7.45 (ddd, J = 8.2, 7.2, 1.2 Hz, 1H, H_3). ^{13}C{^{1}H} NMR (101 MHz, $CDCl_3$): 158.6(C_7), 153.6(C_1), 144.5(C_8), 139.1(C_{10}), 134.8(C_5), 131.5 (q, $J_{C,F}$ = 33.3 Hz, C_{13}), 127.5 (q, $J_{C,F}$ = 3.2 Hz, C_{12} + C_{14}), 126.7(C_4), 125.9 (C_3), 123.6 (q, $J_{C,F}$ = 272.4Hz, C_{16}), 123.2 (C_5), 122.1(C_2), 120.7(C_{11} + C_{15}), 119.9(C_9). ^{19}F{^{1}H} NMR (188 MHz, ACN-d_3): −63.75. HRMS (ESI/Q-TOF) m/z: $[M+H]^+$ Calcd for $C_{16}H_{10}F_3N_4S$ 347.0573; Found 347.0578. HRMS (ESI/Q-TOF) m/z: $[M-2N + H]^+$ Calcd for $C_{16}H_{10}F_3N_2S$ 319.0511; Found 319.0515. HRMS (ESI/Q-TOF) m/z: $[M+Na]^+$ Calcd for $C_{16}H_9F_3N_4SNa$ 369.0392; Found 369.0401. Anal. Calcd for $C_{16}H_9F_3N_4S$: C, 55.49; H, 2.62; N, 16.18; S, 9.26. Found: C, 55.42; H, 2.59; N, 16.05; S, 9.32.

4.8. 2-(1-(4-nitrophenyl)-1H-1,2,3-triazol-4-yl)benzo[d]thiazole (**5d**)

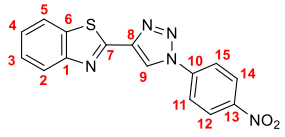

White powder. Yield = 63% (1.02 g). ^{1}H NMR (401 MHz, DMSO-d_6): 9.88 (s, 1H, H_9), 8.51–8.46 (m, 2H, H_{12} + H_{14}), 8.39–8.34 (m, 2H, H_{11} + H_{15}), 8.21 (ddd, J = 8.0, 1.3, 0.6 Hz, 1H, H_2), 8.08 (dt, J = 8.1, 1.0 Hz, 1H, H_5), 7.59 (ddd, J = 8.3, 7.2, 1.2 Hz, 1H, H_4), 7.52 (ddd, J = 8.2, 7.1, 1.2 Hz, 1H, H_3). ^{13}C {^{1}H} NMR (101 MHz, DMSO-d_6): 158.2(C_7), 153.2 (C_1), 147.2(C_{13}), 143.4(C_8), 140.5(C_{10}), 134.0(C_6), 126.9(C_4), 125.9 (C_3), 125.6(C_{12} + C_{14}), 122.8(C_5), 122.7(C_2), 122.6(C_9), 121.2(C_{11} + C_{15}). HRMS (ESI/Q-TOF) m/z: $[M+H]^+$ Calcd for $C_{15}H_{10}N_5O_2S$ 324.0550; Found 324.0562. HRMS (ESI/Q-TOF) m/z: $[M-2N + H]^+$ Calcd for $C_{15}H_{10}N_3O_2S$ 296.0488; Found = 296.0499. HRMS (ESI/Q-TOF) m/z: $[M+Na]^+$ Calcd for $C_{15}H_9N_5O_2SNa$ 346.0369; Found 346.0381. Anal. Calcd for $C_{15}H_9N_5O_2S$: C, 55.72; H, 2.81; N, 21.66; S, 9.92. Found: C, 55.63; H, 2.78; N, 21.63; S, 9.85.

4.9. 2-(1-(4-methoxyphenyl)-1H-1,2,3-triazol-4-yl)benzo[d]thiazole (**5e**)

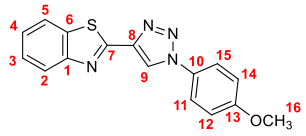

White powder. Yield = 75% (1.16 g). ^{1}H NMR (401 MHz, $CDCl_3$): 8.61 (s, 1H, H_9), 8.06 (d, J = 8.4 Hz, 1H, H_5), 7.98 (d, J = 7.7 Hz, 1H, H_2), 7.75–7.69 (m, 2H, H_{11} + H_{15}), 7.53 (ddd, J = 8.4, 6.8, 1.2 Hz, 1H, H_4), 7.44 (ddd, J = 7.8, 6.8, 1.2 Hz, 1H, H_3), 7.10–7.04 (m, 2H, H_{12} + H_1), 3.90 (s, 3H, H_{16}). ^{13}C{^{1}H} NMR (101 MHz, $CDCl_3$): 160.4(C_{13}), 159.3(C_7), 153.8(C_1), 143.9(C_8), 134.9(C_6), 130.1(C_{10}), 126.6(C_4), 125.6(C_3), 123.1(C_5), 122.4(C_{11} + C_{15}), 122.1(C_2), 120.2(C_9), 115.1 (C_{12} + C_{14}), 55.8(C_{16}). HRMS (ESI/Q-TOF) m/z: $[M+H]^+$ Calcd for

$C_{16}H_{13}N_4OS$ 309.0810; Found 309.0805. HRMS (ESI/Q-TOF) *m/z*: $[M-2N+H]^+$ Calcd for $C_{16}H_{13}N_2OS$ 281.0743; Found 281.0729. HRMS (ESI/Q-TOF) *m/z*: $[M+Na]^+$ Calcd for $C_{16}H_{12}N_4OSNa$ 331.0624; Found 331.0615. Anal. Calcd for $C_{16}H_{12}N_4OS$: C, 62.32; H, 3.92; N, 18.17; S, 10.40. Found: C, 62.35; H, 3.90; N, 18.06; S, 10.48.

4.10. 4-(4-(benzo[d]thiazol-2-yl)-1H-1,2,3-triazol-1-yl)-N,N-dimethylaniline (**5f**)

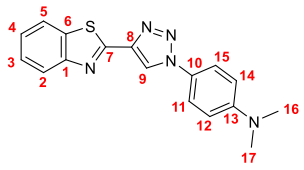

White powder. Yield = 60% (964 mg). ^{1}H NMR (401 MHz, $CDCl_3$): δ 8.58 (s, 1H, H_9), 8.05 (d, J = 8.1 Hz, 1H, H_5), 7.97 (d, J = 7.9 Hz, 1H, H_2), 7.64 (d, J = 8.4 Hz, 2H, H_{11} + H_{15}), 7.52 (m, 1H, H_4), 7.43 (m, 1H, H_3), 6.84 (d, J = 8.5 Hz, 2H, H_{12} + H_{14}), 3.05 (s, 6H, H_{16} + H_{17}). ^{13}C {^{1}H} NMR (101 MHz, $CDCl_3$): 159.7(C_7), 153.7(C_1), 150.8(C_{13}), 143.6 (C_8), 134.8(C_6), 126.5(C_4), 125.5(C_3), 123.0(C_5), 122.08(C_{11} + C_{15}), 122.06(C_2), 120.0(C_9), 112.8(C_{12} + C_{14}), 40.8(C_{16} + C_{17}). HRMS (ESI/Q-TOF) *m/z*: $[M+H]^+$ Calcd for $C_{17}H_{16}N_5S$ 322.1121; Found 322.1128. HRMS (ESI/Q-TOF) *m/z*: $[M-2N+H]^+$ Calcd for $C_{17}H_{16}N_3S$ 294.1060; Found 294.1067. HRMS (ESI/Q-TOF) *m/z*: $[M+Na]^+$ Calcd for $C_{17}H_{15}N_5SNa$ 344.0940; Found 344.0949. Anal. Calcd for $C_{17}H_{15}N_5S$: C, 66.53; H, 4.70; N, 21.79; S, 9.98. Found: C, 65.84; H, 4.74; N, 21.84; S, 10.09.

4.11. 2-(1-(4-nitrophenyl)-1H-1,2,3-triazol-4-yl)-2,3-dihydrobenzo[d]thiazole (**6d**)

Yellow powder. Yield = 87% (1.42 g). ^{1}H NMR (401 MHz, DMSO-d_6): 9.05 (s, 1H), 8.45–8.41 (m, 2H), 8.30–8.20 (m, 2H), 7.11–7.01 (m, 2H), 6.91 (dd, J = 7.6, 1.3 Hz, 1H), 6.70–6.58 (m, 3H). ^{13}C NMR (101 MHz, DMSO-d_6): 151.7(C), 147.1(C), 146.8(C), 140.8(C), 125.5(CH), 124.9(CH), 121.3(CH), 121.2(CH), 120.7(CH), 119.2(CH), 109.5(CH), 60.9(CH_2). HRMS (ESI/Q-TOF) *m/z*: $[M+H]^+$ Calcd for $C_{15}H_{12}N_5O_2S$ 326.0706; Found 326.0706. HRMS (ESI/Q-TOF) *m/z*: $[M-2N+H]^+$ Calcd for $C_{15}H_{12}N_3O_2S$ 298.0645; Found 298.0647. HRMS (ESI/Q-TOF) *m/z*: $[M+Na]^+$ Calcd for $C_{15}H_{11}N_5O_2SNa$ 348.0526; Found 348.0541. Anal. Calcd for $C_{15}H_{11}N_5O_2S$: C, 55.38; H, 3.41; N, 21.53; S, 9.85. Found: C, 55.76; H, 3.38; N, 21.68; S, 9.87.

4.12. X-ray data collection and structure refinement

A specimen of $C_{16}H_9F_3N_4S$ (**5c**), approximate dimensions 0.090 mm × 0.170 mm x 0.200 mm, was used for the X-ray crystallographic analysis. The X-ray intensity data were measured (λ = 0.71073 Å). The integration of the data using a monoclinic unit cell yielded a total of 20733 reflections to a maximum θ angle of 29.29° (0.73 Å resolution), of which 3821 were independent (average redundancy 5.426, completeness = 98.6%, Rint = 3.52%, Rsig = 2.57%) and 3175 (83.09%) were greater than 2σ(F2). The final cell constants of a = 7.369(4) Å, b = 5.705 (3) Å, c = 33.849(19) Å, β = 92.88(5) °, V = 1421.2(13) Å^3, are based upon the refinement of the XYZ-centroids of reflections above 20 σ(I). The calculated minimum and maximum transmission coefficients (based on crystal size) are 0.9480 and 0.9760. The structure was solved and refined using the Bruker SHELXTL Software Package, the final anisotropic full-matrix least-squares refinement on F2 with 217 variables converged at R_1 = 4.73%, for the observed data and wR_2 = 11.74% for all data. The goodness-of-fit was 1.080. The largest peak in the final difference electron density synthesis was 0.861 e$^-$/Å^3 and the largest hole was −0.793 e$^-$/Å^3 with an RMS deviation of 0.080 e$^-$/Å^3.

4.13. Computational details

DFT calculations have been carried out on **5a-f** by using the M06-2X functional [57], with full geometry optimization. The solvent (ACN, DMSO or water) was implicitly considered by using the PCM method [58]. Frequency calculations, in the normal oscillator approximation, were carried out to check that the optimized geometries corresponded to energy minima on the potential energy surface. TD-DFT calculations have been performed using the same methods and models described above, to calculate the electronic absorption spectra of the six compounds **5a-f**. ^{1}H NMR chemical shift values have been calculated by using the GIAO method [59], in ACN solvent, by subtracting the isotropic shift of each compound hydrogen atom to the isotropic shift of one of the twelve equivalent tetramethylsilane hydrogen atoms. All calculations have been performed by the Gaussian16 program package [60].

4.14. Cell culture

HeLa cells were cultured in Dulbecco's Modified Eagle Medium (1 g/L glucose), A2780 cells were cultured in RPMI-1640 media. A549 and CHO cells were maintained in F-12 media. All cell media were supplemented with fetal bovine serum (10% v/v) and 1 mM L-glutamine, and cells were cultured in a CO_2 incubator at 310 K with a subculture routine of 2–3 times a week using an appropriate density for each cell line. Cells were confirmed to be mycoplasma-free using a standard Hoechst staining method.

4.15. Antiproliferative activity assays

Briefly, cells were seeded in 96-well plates at a density of 5000 cells/well in complete medium and incubated for 24 h. Compounds were diluted in serial using sterile DMSO as solvent and added at the final concentrations in the range of 0–100 μM in a final volume of 100 μL per well (final DMSO % < 0.4 v/v). After 48 h of drug exposure, treatment-containing medium was aspirated by suction, cells washed with saline PBS buffer and loaded with 50 μL of MTT solution (1 mg/mL) for additional 4 h. Then the MTT was removed and 50 μL DMSO was added to solubilize the purple formazan crystals formed in active cells. The absorbance was measured at 570 nm using a microplate reader (FLUOstar Omega) and the IC_{50} values were calculated based on the inhibitory rate curves using the next the equation:

$$I = \frac{I_{max}}{1 + \left(\frac{IC_{50}}{C}\right)^n}$$

Where I represent the percentage inhibition of viability observed, Imax is the maximal inhibitory effect, IC_{50} is the concentration that inhibits 50% of maximal growth, C is the concentration of the treatment and n is the slope of the semi-logarithmic dose-response sigmoidal curves. The non-linear fitting was performed using SigmaPlot 14.0 software. All experiments were performed in three independent studies with triplicate points per concentration level (n = 3 biologically independent replicates).

4.16. Microscopy imaging

For contrast-phase microscopy, Zeiss Axio Observer 7 microscope was used to capture images of A2780 and HeLa cells seeded 96-well plates from antiproliferative assays at indicated concentrations. For confocal microscopy imaging, HeLa cells were seeded onto Ibidi μ-slide 4 well at a density of $3{\cdot}10^4$ cells/cm^2 and allowed to attach to cell surface. Cells were treated with **5f** for 1 h at indicated concentrations, washed twice with PBS and imaged under an inverted laser scanning confocal microscope using λ_{exc} = 405 nm (Leica STELLARIS 8). Alternatively, cells were co-stained with MitoTracker Green (MTG; 100 nM)

for 30 min after incubation with the compound.

Accession codes

CCDC 2155202 contains the supplementary crystallographic data for this paper. These data can be obtained free of charge via www.ccdc.cam.ac.uk/data_request/cif, or by emailing data_request@ccdc.cam.ac.uk, or by contacting The Cambridge Crystallographic Data Centre, 12 Union Road, Cambridge CB2 1EZ, UK; fax: +44 1223 336033.

CRediT authorship contribution statement

Francisco J. Ballester: designed, synthesized and characterized the compounds. **Enrique Ortega-Forte:** designed, performed, and interpreted all biological experiments (cytotoxicity and confocal microscopy studies). **Delia Bautista:** determined the crystal structures of the compounds. **M. Dolores Santana:** supervision, designed the research, wrote the manuscript. **Giampaolo Barone:** designed the research, wrote the manuscript, performed and interpreted the theoretical calculations. **José Ruiz:** Resources, designed the research, wrote the manuscript, which was contributed by all authors. All authors have approved the final version of the manuscript.

Declaration of competing interest

The authors declare that they have no known competing financial interests or personal relationships that could have appeared to influence the work reported in this paper.

Data availability

Data will be made available on request.

Acknowledgment

This work was supported by the Spanish Ministerio de Ciencia e Innovación (MCI/AEI) and FEDER funds (Projects PID2021-122850NB-I00 and MultiMetDrugs network RED2018-102471-T), Fundación Séneca-Región de Murcia (Project 20857/PI/18). E.O. thanks AECC (PRDMU19003ORTE). Francisco José Ballester thanks Fundación Séneca-Región de Murcia (20277/FPI/17). G.B. gratefully acknowledges the CINECA award N. IsC93, year 2021, under the ISCRA initiative, for the availability of high-performance computing resources and support.

Appendix A. Supplementary data

Supplementary data to this article can be found online at https://doi.org/10.1016/j.dyepig.2022.110905.

References

[1] Klymchenko AS. Solvatochromic and fluorogenic dyes as environment-sensitive probes: design and biological applications. Acc Chem Res 2017;50(2):366–75. https://doi.org/10.1021/acs.accounts.6b00517.
[2] Nociarová J, Osuský P, Rakovský E, Georgiou D, Polyzos I, Fakis M, Hrobárik P. Direct iodination of electron-deficient benzothiazoles: rapid access to two-photon absorbing fluorophores with quadrupolar D-π-A-π-D architecture and tunable heteroaromatic core. Org Lett 2021;23(9):3460–5. https://doi.org/10.1021/acs.orglett.1c00893.
[3] Safir Filho M, Fiorucci S, Martin AR, Benhida R. Design, synthesis and photophysical studies of styryl-based push-pull fluorophores with remarkable solvatofluorochromism. New J Chem 2017;41(22):13760–72. https://doi.org/10.1039/C7NJ03142D.
[4] Hrobárik P, Hrobáriková V, Sigmundová I, Zahradník P, Fakis M, Polyzos I, Persephonis P. Benzothiazoles with tunable electron-withdrawing strength and reverse polarity: a route to triphenylamine-based chromophores with enhanced two-photon absorption. J Org Chem 2011;76(21):8726–36. https://doi.org/10.1021/jo201411t.
[5] Bureš F. Fundamental aspects of property tuning in push-pull molecules. RSC Adv 2014;4(102):58826–51. https://doi.org/10.1039/C4RA11264D.
[6] Chander Sharma P, Sharma D, Sharma A, Bansal KK, Rajak H, Sharma S, Thakur VK. New horizons in benzothiazole scaffold for cancer therapy: advances in bioactivity, functionality, and chemistry. Appl Mater Today 2020;20:100783. https://doi.org/10.1016/j.apmt.2020.100783.
[7] Stevens MFG, McCall CJ, Lelievald P, Alexander P, Richter A, Davies DE. Structural studies on bioactive compounds. 23. Synthesis of polyhydroxylated 2-phenylbenzothiazoles and a comparison of their cytotoxicities and pharmacological properties with genistein and quercetin. J Med Chem 1994;37(11):1689–95. https://doi.org/10.1021/jm00037a020.
[8] Bradshaw T, Stevens MF, Westwell A. The discovery of the potent and selective antitumour agent 2-(4-amino-3-Methylphenyl)Benzothiazole (DF 203) and related compounds. Comput Mater Continua (CMC) 2001;8(2):203–10. https://doi.org/10.2174/0929867013373714.
[9] Irfan A, Batool F, Zahra Naqvi SA, Islam A, Osman SM, Nocentini A, Alissa SA, Supuran CT. Benzothiazole derivatives as anticancer agents. J Enzym Inhib Med Chem 2020;35(1):265–79. https://doi.org/10.1080/14756366.2019.1698036.
[10] Pathak N, Rathi E, Kumar N, Kini SG, Rao CM. A review on anticancer potentials of benzothiazole derivatives. MRMC 2020;20(1):12–23. https://doi.org/10.2174/1389557519666190617153213.
[11] Keri RS, Patil MR, Patil SA, Budagumpi S. A comprehensive review in current developments of benzothiazole-based molecules in medicinal chemistry. Eur J Med Chem 2015;89:207–51. https://doi.org/10.1016/j.ejmech.2014.10.059.
[12] Shi D-F, Bradshaw TD, Wrigley S, McCall CJ, Lelieveld P, Fichtner I, Stevens MFG. Antitumor benzothiazoles. 3. Synthesis of 2-(4-Aminophenyl)Benzothiazoles and evaluation of their activities against breast cancer cell lines *in vitro* and *in vivo*. J Med Chem 1996;39(17):3375–84. https://doi.org/10.1021/jm9600959.
[13] Hai Nam N, Thi Phuong Dung P, Thien Thuong P. Synthesis and biological evaluation of a series of 2-(substitutedphenyl) benzothiazoles. MC 2011;7(2):127–34. https://doi.org/10.2174/157340611794859361.
[14] Choi S-J, Park HJ, Lee SK, Kim SW, Han G, Choo H-YP. Solid phase combinatorial synthesis of benzothiazoles and evaluation of topoisomerase II inhibitory activity. Bioorg Med Chem 2006;14(4):1229–35. https://doi.org/10.1016/j.bmc.2005.09.051.
[15] Palmer PJ, Trigg RB, Warrington JV. Benzothiazolines as antituberculous agents. J Med Chem 1971;14(3):248–51. https://doi.org/10.1021/jm00285a022.
[16] Yildiz-Oren I, Yalcin I, Aki-Sener E, Ucarturk N. Synthesis and structure-activity relationships of new antimicrobial active multisubstituted benzazole derivatives. Eur J Med Chem 2004;39(3):291–8. https://doi.org/10.1016/j.ejmech.2003.11.014.
[17] Sharma PC, Sinhmar A, Sharma A, Rajak H, Pathak DP. Medicinal significance of benzothiazole scaffold: an insight view. J Enzym Inhib Med Chem 2013;28(2):240–66. https://doi.org/10.3109/14756366.2012.720572.
[18] Watanabe H, Ono M, Ariyoshi T, Katayanagi R, Saji H. Novel benzothiazole derivatives as fluorescent probes for detection of β-amyloid and α-synuclein aggregates. ACS Chem Neurosci 2017;8(8):1656–62. https://doi.org/10.1021/acschemneuro.6b00450.
[19] Klunk WE, Wang Y, Huang G, Debnath ML, Holt DP, Mathis CA. Uncharged thioflavin-T derivatives bind to amyloid-beta protein with high affinity and readily enter the brain. Life Sci 2001;69(13):1471–84. https://doi.org/10.1016/S0024-3205(01)01232-2.
[20] Lockhart A, Ye L, Judd DB, Merritt AT, Lowe PN, Morgenstern JL, Hong G, Gee AD, Brown J. Evidence for the presence of three distinct binding sites for the thioflavin T class of alzheimer's disease PET imaging agents on β-amyloid peptide fibrils. J Biol Chem 2005;280(9):7677–84. https://doi.org/10.1074/jbc.M412056200.
[21] Herrera Cano N, Ballari MS, López AG, Santiago AN. New synthesis and biological evaluation of benzothiazole derivates as antifungal agents. J Agric Food Chem 2015;63(14):3681–6. https://doi.org/10.1021/acs.jafc.5b00150.
[22] Ammazzalorso A, Carradori S, Amoroso R, Fernández IF. 2-Substituted benzothiazoles as antiproliferative agents: novel insights on structure-activity relationships. Eur J Med Chem 2020;207:112762. https://doi.org/10.1016/j.ejmech.2020.112762.
[23] Boechat N, Ferreira VF, Ferreira SB, Ferreira M de LG, da Silva F de C, Bastos MM, Costa M dos S, Lourenço MCS, Pinto AC, Krettli AU, Aguiar AC, Teixeira BM, da Silva NV, Martins PRC, Bezerra FAFM, Camilo ALS, da Silva GP, Costa CCP. Novel 1,2,3-triazole derivatives for use against *Mycobacterium tuberculosis* H37Rv (ATCC 27294) strain. J Med Chem 2011;54(17):5988–99. https://doi.org/10.1021/jm2003624.
[24] Kaushik CP, Pahwa A. Convenient synthesis, antimalarial and antimicrobial potential of thioethereal 1,4-disubstituted 1,2,3-triazoles with ester functionality. Med Chem Res 2018;27(2):458–69. https://doi.org/10.1007/s00044-017-2072-x.
[25] Madasu C, Karri S, Sangaraju R, Sistla R, Uppuluri MV. Synthesis and biological evaluation of some novel 1,2,3-triazole hybrids of myrrhanone B isolated from commiphora mukul gum resin: identification of potent antiproliferative leads active against prostate cancer cells (PC-3). Eur J Med Chem 2020;188:111974. https://doi.org/10.1016/j.ejmech.2019.111974.
[26] Alam MM. 1,2,3-Triazole hybrids as anticancer agents: a review. Arch Pharmazie 2022;355(1):2100158. https://doi.org/10.1002/ardp.202100158.
[27] Safavi M, Ashtari A, Khalili F, Mirfazli SS, Saeedi M, Ardestani SK, Rashidi Ranjbar P, Barazandeh Tehrani M, Larijani B, Mahdavi M. Novel quinazolin-4(3*H*)-One linked to 1,2,3-triazoles: synthesis and anticancer activity. Chem Biol Drug Des 2018;92(1):1373–81. https://doi.org/10.1111/cbdd.13203.
[28] Bozorov K, Zhao J, Aisa HA. 1,2,3-Triazole-Containing hybrids as leads in medicinal chemistry: a recent overview. Bioorg Med Chem 2019;27(16):3511–31. https://doi.org/10.1016/j.bmc.2019.07.005.

[29] Trouvé J, Zardi P, Al-Shehimy S, Roisnel T, Gramage-Doria R. Enzyme-like supramolecular iridium catalysis enabling C-H bond borylation of pyridines with *meta* -selectivity. Angew Chem Int Ed 2021;60(33):18006–13. https://doi.org/10.1002/anie.202101997.

[30] Crowley JD, McMorran DA. "Click-Triazole" coordination chemistry: exploiting 1,4-disubstituted-1,2,3-triazoles as ligands. In: Košmrlj J, editor. Click triazoles. Topics in heterocyclic chemistry, vol. 28. Berlin, Heidelberg: Springer Berlin Heidelberg; 2012. p. 31–83. https://doi.org/10.1007/7081_2011_67.

[31] Schulze B, Schubert US. Beyond click chemistry - supramolecular interactions of 1,2,3-triazoles. Chem Soc Rev 2014;43(8):2522. https://doi.org/10.1039/c3cs60386e.

[32] Zabarska N, Stumper A, Rau S. CuAAC click reactions for the design of multifunctional luminescent ruthenium complexes. Dalton Trans 2016;45(6):2338–51. https://doi.org/10.1039/C5DT04599A.

[33] Kantheti S, Narayan R, Raju KVSN. The impact of 1,2,3-triazoles in the design of functional coatings. RSC Adv 2015;5(5):3687–708. https://doi.org/10.1039/C4RA12739K.

[34] Merkt FK, Pieper K, Klopotowski M, Janiak C, Müller TJJ. Sequential Cu-catalyzed four- and five-component syntheses of luminescent 3-triazolylquinoxalines. Chem Eur J 2019;25(40):9447–55. https://doi.org/10.1002/chem.201900277.

[35] Surendra Reddy G, Ramachary DB. Reaction engineering and photophysical studies of fully enriched *C* -Vinyl-1,2,3-Triazoles. Org Chem Front 2019;6(21):3620–8. https://doi.org/10.1039/C9QO00864K.

[36] Schwarze T, Müller H, Ast S, Steinbrück D, Eidner S, Geißler F, Kumke MU, Holdt H-J. Fluorescence lifetime-based sensing of sodium by an optode. Chem Commun 2014;50(91):14167–70. https://doi.org/10.1039/C4CC06112H.

[37] Schwarze T, Riemer J, Müller H, John L, Holdt H, Wessig P. Na $^{+}$ selective fluorescent tools based on fluorescence intensity enhancements, lifetime changes, and on a ratiometric response. Chem Eur J 2019;25(53):12412–22. https://doi.org/10.1002/chem.201902536.

[38] Parent M, Mongin O, Kamada K, Katan C, Blanchard-Desce M. New chromophores from click chemistry for two-photon absorption and tuneable photoluminescence. Chem Commun 2005;15:2029. https://doi.org/10.1039/b419491h.

[39] Brunel D, Dumur F. Recent advances in organic dyes and fluorophores comprising a 1,2,3-triazole moiety. New J Chem 2020;44(9):3546–61. https://doi.org/10.1039/C9NJ06330G.

[40] Jarowski PD, Wu Y-L, Schweizer WB, Diederich F. 1,2,3-Triazoles as conjugative π-linkers in push-pull chromophores: importance of substituent positioning on intramolecular charge-transfer. Org Lett 2008;10(15):3347–50. https://doi.org/10.1021/ol801253z.

[41] Zych D, Slodek A. Acceptor-π-Acceptor-Acceptor/Donor systems containing dicyanovinyl acceptor group with substituted 1,2,3-triazole motif - synthesis, photophysical and theoretical studies. J Mol Struct 2020;1204:127488. https://doi.org/10.1016/j.molstruc.2019.127488.

[42] Zych D, Slodek A, Zimny D, Golba S, Malarz K, Mrozek-Wilczkiewicz A. Influence of the substituent D/A at the 1,2,3-triazole ring on novel terpyridine derivatives: synthesis and properties. RSC Adv 2019;9(29):16554–64. https://doi.org/10.1039/C9RA02655J.

[43] Zych D, Slodek A, Krompiec S, Malarz K, Mrozek-Wilczkiewicz A, Musiol R. 4'-Phenyl-2,2':6',2''-Terpyridine derivatives containing 1-substituted-2,3-triazole ring: synthesis, characterization and anticancer activity. ChemistrySelect 2018;3(24):7009–17. https://doi.org/10.1002/slct.201801204.

[44] Pokhodylo NT, Matiychuk VS, Obushak NB. Synthesis of 1H-1,2,3-Triazole derivatives by the cyclization of aryl azides with 2-benzothiazolylacetonone, 1,3-benzo-thiazol-2-Ylacetonitrile, and (4-aryl-1,3-thiazol-2-Yl)Acetonitriles. Chem Heterocycl Compd 2009;45(4):483–8. https://doi.org/10.1007/s10593-009-0287-6.

[45] Lapina VA, Pavich TA, Pershukevich PP, Trofimov AV, Trofimova NN, Tsaplev YB, Zak PP. Exploring the utility of coumarins-based luminescent spectra converters. J Phys Org Chem 2017;30(9):e3731. https://doi.org/10.1002/poc.3731.

[46] Allen FH, Kennard O, Watson DG, Brammer L, Orpen AG, Taylor R. Tables of bond lengths determined by X-ray and neutron diffraction. Part 1. Bond lengths in organic compounds. J Chem Soc 1987;2(12):S1. https://doi.org/10.1039/p298700000s1.

[47] Pyykkö P, Atsumi M. Molecular single-bond covalent radii for elements 1-118. Chem Eur J 2009;15(1):186–97. https://doi.org/10.1002/chem.200800987.

[48] Allen FH. The Cambridge structural database: a quarter of a million crystal structures and rising. Acta Crystallogr B Struct Sci 2002;58(3):380–8. https://doi.org/10.1107/S0108768102003890.

[49] Wang K, Huang S, Zhang Y, Zhao S, Zhang H, Wang Y. Multicolor fluorescence and electroluminescence of an ICT-type organic solid tuned by modulating the accepting nature of the central core. Chem Sci 2013;4(8):3288. https://doi.org/10.1039/c3sc51091c.

[50] Wan W, Wang H, Lin H, Wang J, Jiang Y, Jiang H, Zhu S, Wang Z, Hao J. Synthesis, electrochemical, photophysical, and electroluminescent properties of organic dyes containing pyrazolo[3, 4-b]Quinoline chromophore. Dyes Pigments 2015;121:138–46. https://doi.org/10.1016/j.dyepig.2015.05.002.

[51] Chen M, Chen D, Chou P. Fluorescent chromophores containing the nitro group: relatively unexplored emissive properties. ChemPlusChem 2021;86(1):11–27. https://doi.org/10.1002/cplu.202000592.

[52] Slodek A, Zych D, Maroń A, Gawecki R, Mrozek-Wilczkiewicz A, Malarz K, Musioł R. Phenothiazine derivatives - synthesis, characterization, and theoretical studies with an emphasis on the solvatochromic properties. J Mol Liq 2019;285:515–25. https://doi.org/10.1016/j.molliq.2019.04.102.

[53] Bhattacharyya Kankan, Chowdhury Mihir. Environmental and magnetic field effects on exciplex and twisted charge transfer emission. Chem Rev 1993;93(1):507–35. https://doi.org/10.1021/cr00017a022.

[54] Kucherak OA, Didier P, Mély Y, Klymchenko AS. Fluorene analogues of prodan with superior fluorescence brightness and solvatochromism. J Phys Chem Lett 2010;1(3):616–20. https://doi.org/10.1021/jz9003685.

[55] Hong Y, Lam JWY, Tang BZ. Aggregation-induced emission: phenomenon, mechanism and applications. Chem Commun 2009;29:4332. https://doi.org/10.1039/b904665h.

[56] Fletcher JT, Christensen JA, Villa EM. Tandem synthesis of 1-formyl-1,2,3-triazoles. Tetrahedron Lett 2017;58(47):4450–4. https://doi.org/10.1016/j.tetlet.2017.10.023.

[57] Rassolov VA, Ratner MA, Pople JA, Redfern PC, Curtiss LA. 6-31G* basis set for third-row atoms. J Comput Chem 2001;22(9):976–84. https://doi.org/10.1002/jcc.1058.

[58] Tomasi J, Mennucci B, Cammi R. Quantum mechanical continuum solvation models. Chem Rev 2005;105(8):2999–3094. https://doi.org/10.1021/cr9904009.

[59] Cheeseman JR, Trucks GW, Keith TA, Frisch MJ. A comparison of models for calculating nuclear magnetic resonance shielding tensors. J Chem Phys 1996;104(14):5497–509. https://doi.org/10.1063/1.471789.

[60] Frisch MJ, Trucks GW, Schlegel HB, Scuseria GE, Robb MA, Cheeseman JR, Scalmani G, Barone V, Petersson GA, Nakatsuji H, Li X, Caricato M, Marenich AV, Bloino J, Janesko BG, Gomperts R, Mennucci B, Hratchian HP, Ortiz JV, Izmaylov AF, Sonnenberg JL, Williams-Young D, Ding F, Lipparini F, Egidi F, Goings J, Peng B, Petrone A, Henderson T, Ranasinghe D, Zakrzewski VG, Gao J, Rega N, Zheng G, Liang W, Hada M, Ehara M, Toyota K, Fukuda R, Hasegawa J, Ishida M, Nakajima T, Honda Y, Kitao O, Nakai H, Vreven T, Throssell K, Montgomery Jr, Peralta JE, Ogliaro F, Bearpark MJ, Heyd JJ, Brothers EN, Kudin, Staroverov, Keith TA, Kobayashi R, Normand J, Raghavachari JK, Rendell AP, Burant JC, Iyengar SS, Tomasi J, Cossi M, Millam JM, Klene M, Adamo C, Cammi R, Ochterski JW, Martin RL, Morokuma K, Farkas O, Foresman JB, Fox DJ. Gaussian 16, revision C.016. 2019.